Target current: a useful parameter for characterizing laser ablation

J. KRÁSA,[1,*] E. GIUFFREDA,[2,3] D. DELLE SIDE,[2,3] V. NASSISI,[2,3] D. KLÍR,[4,5] J. CIKHARDT,[4,5] AND K. ŘEZÁČ[4,5]

[1]Institute of Physics, CAS, Prague, Czech Republic
[2]Dipartimento di Matematica e Fisica "Ennio De Giorgi", Università del Salento, Lecce, Italy
[3]INFN, Sezione di Lecce, Italy
[4]Faculty of Electrical Engineering, Czech Technical University in Prague, Czech Republic
[5]Institute of Plasma Physics, CAS, Prague, Czech Republic

Abstract

A current flowing between the ground and target exposed to the nanosecond laser radiation is analyzed to complete characteristics of laser ablation. Three phases of the target current are distinguished. During the ignition phase, the electron emission is driven by the laser pulse and the positive charge generated on the target is balanced by electrons coming from the ground through the target holder. At post-pulse times, a peaked waveform of the target current is typical for the active phase of the plasma and can give information on the material composition of the ablated surface layers. The afterglow phase is determined by a current of electrons flowing from the target to the ground. Experiment shows that the time-resolved target current is very sensitive to the actual composition of the surface layer of irradiated target and laser parameters.

Keywords: Impurities on target surface; Positive and negative target polarization; Space structure of ion front; Target current in laser-produced plasmas

1. INTRODUCTION

The target polarization by laser ablation starts when the most energetic electrons escape a potential barrier and leave the target (Benjamin *et al.*, 1979; Dubois *et al.*, 2014; Poyè *et al.*, 2015). The charge on the target generated by escaped electrons is balanced by a return target current $I_T(t)$ coming from the ground through the holder assembly to neutralize it. The waveform and amplitude of $I_T(t)$ depend on initial laser–target interaction (Cikhardt *et al.*, 2014; Krása *et al.*, 2015; Poyè *et al.*, 2015). Theoretical modelling of the target polarization by femto- and picosecond laser interaction predicts an independence of the generated charge on the target material (Poyè *et al.*, 2015). Furthermore, the waveform of $I_T(t)$ occurred at the few picosecond time scale can be strongly deformed by the oscilloscope bandwidth as well as by the target size and the support assembly, the impedance and capacity of which create an electric circuit causing the nanosecond oscillations of the target charge (Dubois *et al.*, 2014).

Contrary to this result, experiments on the low intensity laser pulse–target interaction with nanosecond duration demonstrated that the target current depends on the target material and can last up to tens of microsecond (Cikhardt *et al.*, 2014; Krása *et al.*, 2015). An experiment with 300-ps laser beam delivering the intensity of 10^{16} W/cm^2 onto a target shown that the duration of $I_T(t)$ is also much longer than the laser pulse duration τ_{FWHM} (Cikhardt *et al.*, 2014). In this case the $I_T(t)$ reached a maximum value of several kA.

The analysis of both the return target currents and ion emission by laser ablation reveals various charging regimes depending on the target and laser parameters. It allows for identification of the relevant phenomena associated with laser–matter interaction and, thus, completing analytical methods based on the plasma ablation.

2. EXPERIMENTAL ARRANGEMENT

The experimental configuration consists of a vacuum chamber, where the target is placed, and detection devices finalized for the characterization of laser-produced plasmas. The plasma was produced with the use of two different

---

*Address correspondence and reprint requests to: J. Krása, Institute of Physics, CAS, Prague, Czech Republic. E-mail: krasa@fzu.cz

1

lasers: 300-ps laser system PALS operating at 1315 nm, which delivers an intensity up to 5×10^{16} W/cm^2 on targets, and a 23-ns Compex 205 krypton fluoride (KrF) excimer laser operating at 248 nm which delivers an intensity up to 10^{10} W/cm^2. The target holder was connected to the ground either directly and the target current was measured with an inductive probe when the PALS laser generated very high currents (Cikhardt *et al.*, 2014), or through resistors, as Figure 1 shows for the plasma produced with the low intensity KrF excimer laser.

The emission of ions by laser-produced plasmas was observed with the use of Faraday cups. To obtain a space distribution of ion charge density $q(x,\tau)$ in C/cm^3 at an arbitrary chosen instant τ from the laser–target interaction, the ion current density $j_{FC}(L,t)$ in A/cm^2, detected at distance L from the target, was transformed to the distance-of-flight (DOF) spectra using a relationship:

$$q(x, t) = j_{FC}(x)tL^3/x^4, \tag{1}$$

where $x = L\,\tau/t$ (Krása *et al.*, 2014).

3. RESULTS AND DISCUSSION

Ionized species being contained in ablated target mass expand into the vacuum with a velocity which is proportional to the focused laser intensity, whereas their amount is mainly proportional to the delivered fluence. The high-power nanosecond lasers produce a plasma causing the target current, as Figure 2 shows for C and Au foil targets irradiated by 433-J and 487-J energy, respectively, delivered by the laser system PALS. Figure 2a shows the time derivative of the target current $dI_T(t)/dt$ obtained with the use of the inductive probe, and Figure 2b shows $I_T(t)$, which reaches a *kA level*. $I_T(t)$ it is modulated in time with both the target-holder electric circuit and vacuum chamber (i.e. resonator) forcing the space charge to ring at their natural frequencies (De Marco *et al.*, 2016). Although this fact makes it difficult to identify the influence of target elements on the return current, it allows us to identify two phases of the return current. The first one, that is, the ignition phase, is related to the laser–matter interaction, and its duration, $t_{L-0.1}$, is given by the full width at one-tenth of maximum of the laser pulse, as Figure 2a indicates.
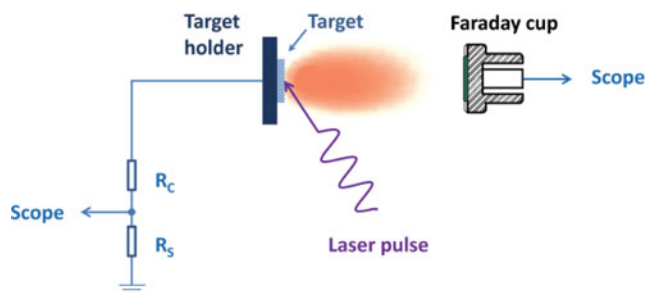

Fig. 1. Sketch of the experimental setup; $R_C = 60\ \Omega$, $R_S = 50\ \Omega$.

It is evident that the time scale of the ignition phase can be much smaller than the time-scale of the liquid phase in the target and its resolidification (Bogaerts *et al.*, 2003). The second phase, that is, the active one during which the positive target polarization continues, can be related to the plasma expansion through the vacuum chamber to the grounded walls, as it will be discussed later.

In contrary to the mass ablation by high-power lasers, the first analysis of the return target current generated by low intensity KrF excimer laser clearly shows the influence of the target composition on the waveform of the target current (Krása *et al.*, 2015). Figure 3 shows both the laser pulse intensity and current from Au and C targets to the ground. Although the target currents start in the ignition phase, which ranges from zero to $t_{L-0.1}$, its partial maxima occur in the active phase after the termination of the interaction with laser pulse. The time period of the active phase ranges from $t_{L-0.1}$ to time t_{T-0} at which the target current changes its polarity, that is, $I_T(t_{T-0}) = 0$, and electrons start to flow from the target to the ground. This last phase can be called the afterglow. The duration of the active phase and afterglow depends on the target composition, as the crosshatch patterns indicate for both the Au and C targets in Figure 3. Moreover, the $I_T(t)$ from the graphite target clearly reveals the effect of impurities chemisorbed on the Au-target surface on the laser ablation due to the similarity in $I_T(t)$ waveforms up to $\sim$400 ns. Although the active phase of the C plasma terminates at $\sim$700 ns, the active phase of the Au plasma continues up to $\sim$1.1 µs. This could allow for analyzing the target composition of the $I_T(t)$, as it will be discussed latter.

Variations in the target current spanning the microsecond scale indicate that the target current depends on the expansion of ions through the vacuum chamber, as one may deduce from Figure 4. The current of ions detected with the use of a Faraday cup was transformed to the DOF spectra of ion charge density using the relationship (1). The ion charge density decreases with increasing DOF and time due to the rarefaction of plasma caused by its expansion into the vacuum chamber. The crosshatch pattern demarcates a range from shortest to longest distances from the target to the vacuum chamber walls. It is evident that the $I_T(t)$ reaches the absolute maximum at $t =$ 0.17 and 1.1 µs for C and Au target, respectively, (see Fig. 3) when the plasma is filling only a part of the chamber volume because the DOF of the fastest ions is about 2 and 5.5 cm for C and Au plasma, respectively, while the shortest chamber size is $\approx$10 cm and the longest one is $\approx$28 cm. In this experiment, the $I_T(t)$ reaches a minimum when the fastest ions hit the walls.

The analysis of values of t_{peak}, at which $I_T(t)$ reaches partial maxima for various ionized target elements, including protons and products created by recombination of ionized radicals, gave a linear dependence of t_{max} on square root of mass number A of ions per their charge number Z (Krása *et al.*, 2015):

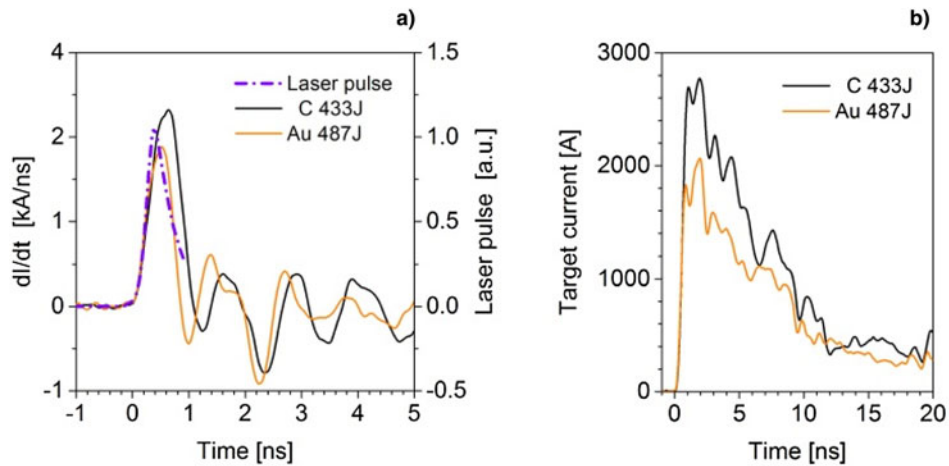$$t_{max} = \alpha + \beta\sqrt{A/Z}. \tag{2}$$

Fig. 2. (a) Comparison of laser intensity with time derivative of currents flowing from C and Au targets to ground and (b) corresponding currents produced with the laser system PALS.

This relationship was derived on the assumption that the value of voltage V_0 accelerating ions to the kinetic energy of $E_{\mathrm{ions}} = eZV_0$ is the same for all the ionized species produced under the same conditions, and that the partial maxima in $I_T(t)$ at t_{max} take place. The fit of (2) to experimental data allows for calculating the path x_{cr} passed by expanding ions at t_{max}. This distance from the target depends on the ion mass M as $x_{\mathrm{cr}} \sim \sqrt{1/M}$.

Another parameter characterizing the target polarization is the current amplitude. It is a measure of the separation of charges, that is, electrons and positive ions being separated into three distinct zones: the first positive layer of charge σ per unit surface is around the position, where the expansion starts; the second positive layer of the same charge σ is on the front of the expanding ions just behind a negative layer of the electron cloud having 2σ charge, as it was derived for a collisionless plasma (Mora, 2003). The charge separation generates a Coulomb force, which affects the velocity distribution of expanding ions by creation of the center-of-mass (CM) velocity via electrical field generated inside the plasma. The shifted Maxwell–Boltzmann velocity distribution $f(\vec{v} - \vec{u}_{CM})$ can be used for characterization of the

plasma expansion (Krása *et al.*, 2011). Then a partial current j_i of ionized species constituting the total ion current $j_{\mathrm{FC}} = \Sigma\, j_i$ detected with a Faraday cup is proportional to:

$$j_i \approx L^2 t^{-5} \exp\left\{ -\frac{m_i}{kT_i}\left(\frac{L}{t} - u_{iCM}\right) \right\}, \qquad (3)$$

where m_i, T_i, and $u_{i\mathrm{CM}}$ are the mass, temperature and CM velocity, respectively, of an ionized species i, and k is the Boltzmann constant. The relationship (3) was derived under assumption that ions are "frozen", because the collisions among particles are insignificant due to the high degree of plasma rarefaction. We note that (3) allows us also to verify if the employed ion probe is positioned outside the recombination zone.

The time derivative dI_T/dt, that is, the rate of change of $I_T(t)$ makes it possible to localize hot regions, where the ion acceleration is formed. Figure 5 shows the time derivative of a target current, which is primarily formed by the acceleration of various ionized species and rarefaction during their expansion into the vacuum, while the influence of the target-holder electric circuit on the current is much weaker. The dI_T/dt shows much more fine structure than $I_T(t)$ and it highlights the influence of impurities on laser ablation and plasma acceleration, as the first two highest peaks of dI_T/dt indicate in Figure 5. This happens in the ignition phase on ns-time scale. On the contrary, the heavy Au ions are accelerated on a time scale of a few hundred nanoseconds what decreases the corresponding part of dI_T/dt although the contribution of Au ions to the I_T is dominant (see Fig. 3).

The influence of light elements on the target polarization is shown in Figure 6 for copper/beryllium alloy target containing Be 1.7–1.9%, and admixtures of Ni and Co. The highest effect of the 2%-amount of Be in the CuBe2% target occurs during the ignition phase, where the target current increases by a factor of ≈2. Moreover, the increase in the target current continues during the active phase, where the
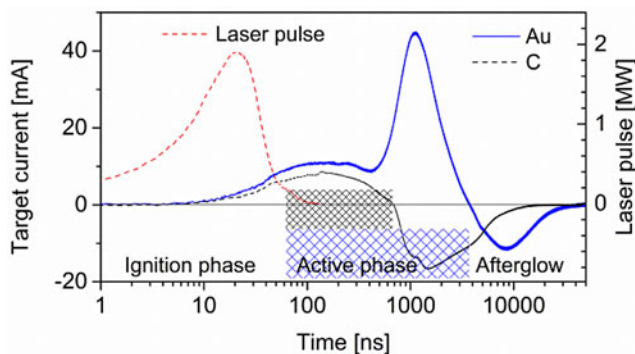

Fig. 3. Time-resolved current flowing from Au and C targets to ground and waveform of KrF excimer laser pulse irradiating target with fluence of 1.2 J/cm².
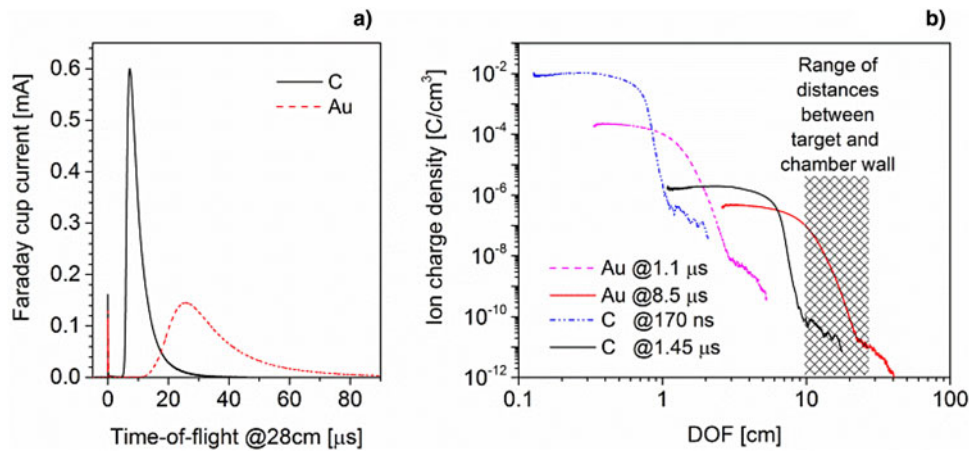
Fig. 4. (a) Current of Au and C ions detected with a Faraday cup at a distance of 28 cm from the target. (b) DOF spectra calculated with (1) for chosen times of 0.17, 1.1, 1.45, and 8. 5 μs after the laser–target interaction.

target polarization by Cu ions is higher by a factor of ≈1.2. Similar effect was observed by analyzing the Faraday cup signal. It was revealed that the Cu plasma containing a small amount of admixture (2% of Be or 4% of Sn) exhibits an enhancement in the charge carried by ions by a factor up to 1.5 and a decrease in the width of plasma plume with respect to the laser-produced pure Cu plasma. This admixture effect on the ion emission was already observed by Fe and Si−2 mass% laser-produced plasmas and was ascribed to the decrease in the recombination efficiency during the plasma expansion (Krása *et al.*, 2008). The results can be completed by the time resolved positive charges occurred in the Cu and CuBe2% targets, as Figure 7 shows. It is evident that the 2% admixture of Be increases the target charge, which was calculated by integration of $I_T(t)$ up to t_{T-0}, where $I_T(t_{T-0}) = 0$.

Both the total positive and negative charges occurring in the active and afterglow phases, respectively, depend on the laser energy, as Figure 8 shows for the tin plasma. Figure 8a shows also variations in the target current caused by acceleration of light elements chemisorbed on the
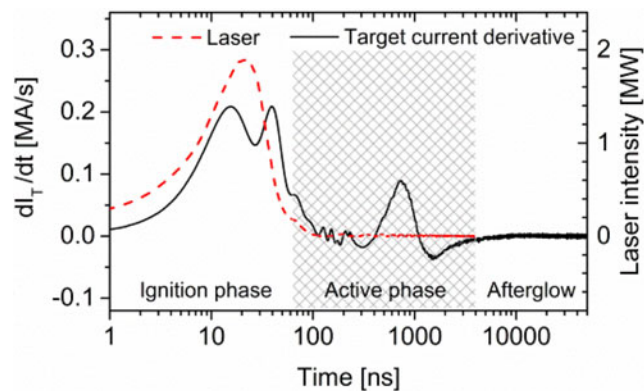
Sn-foil surface (peaks at 70–270 ns). The target polarization evidently depends on the surface contamination level, as the full and dash–dot–dot lines show for the fully developed layer of impurities ablated by the first laser shot or partially developed layer of contaminants during ≈ 1 s after the 1st laser shot, respectively. It seems that just the surface quality significantly contributes to the fluctuations in the shot-to-shot reproducibility in the laser ablation, including the main contribution by heavier species to the target current, as a peak at ≈950 ns caused by Sn ions reveals in Figure 8a.

Figure 8 shows that the duration of $I_T(t) < 0$ is the longest period of the target polarization, and the number of collected electrons is higher than the number of emitted electrons. In this case, the actual plasma should have considerably different properties than do the former plasma. The interpretation of this new phenomenon should also consider the target
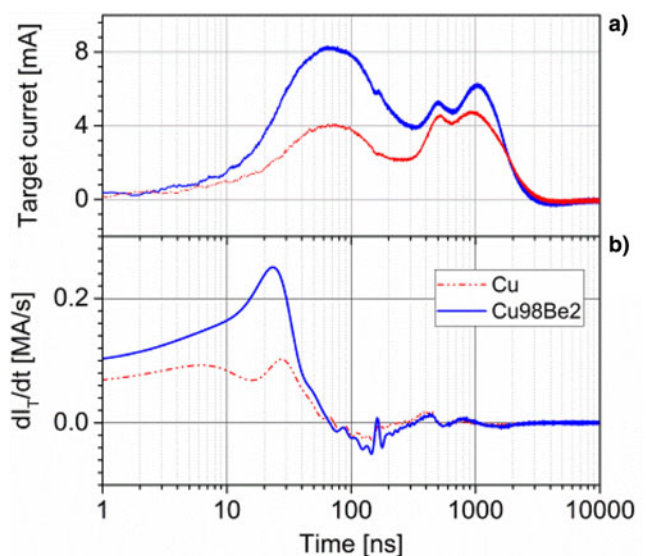

Fig. 5. Time derivative of current flowing from Au target to ground, see Figure 3, and waveform of KrF excimer laser pulse.

Fig. 6. Comparison of currents from Cu and Cu98Be2-alloy targets to ground (a) and time derivative of currents (b).

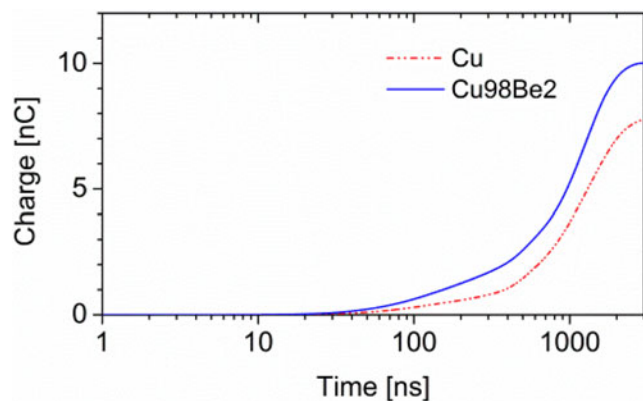**Fig. 7.** Charge generated on Cu and Cu98Be2-alloy targets.

Fig. 9. Time-resolved current flowing from PED target to ground and waveform of KrF excimer laser pulse irradiating target with fluence of 1.2 J/cm^2.

and its holder as a specific Langmuir probe biased to zero voltage (Weaver *et al.*, 1999). The new plasma properties could be related to the group of slowest ions occupying the tail of the time-of-flight (TOF) spectra, which do not exhibit a motion caused by the electric force, that is, $u_{iCM} = 0$ in (3), because they are produced by ionization of ablated neutrals by radiation from laser-produced plasma (Krása *et al.*, 2015). Both the negative amplitude of $I_T(t)$ and its duration depend on target material: the smallest afterglow was observed by the Cu plasma, while the Au plasma revealed one of the dominated afterglows.

An interesting features of the laser ablation is the nature and dynamics of the electric pulse produced inside a plastic target and its correlation to the ion emission (Giuffreda *et al.*, 2016). Figure 9 shows a negative current flowing from a deuterated polyethylene (PED) plastic target to the ground already during the ignition period. This current implies a role of target electrons heated with the laser pulse in plastic insulators. The electrons absorbing the 248-nm laser radiation and also the plasma radiation are liberated in the target via internal photoemission. If the target is thin, these
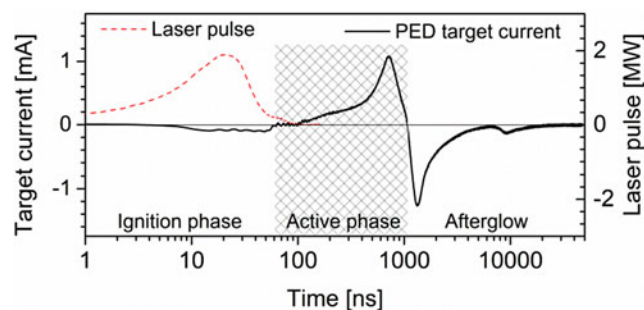
photoelectrons can diffuse to the metallic target holder and flow to the ground. Since the internal photoemission is a volume effect, this partial target current depends on the target/holder surface ratio (Giuffreda *et al.*, 2016).

The observation of the target polarization by laser ablation makes it easy to find information on the plasma formation mainly for ns-pulsed laser–matter interaction, where the laser energy is turned into heat, especially for metals (Bogaerts *et al.*, 2003). Our experiments confirm that the temperature of the evaporated material is sufficiently high during the laser–target interaction in so far that the vapor is ionized and the plasma expands, as for example, Figure 5 shows for metals. As for the PED plastic target (see Fig. 9), the early negative target polarization can be interpreted as a result of the interference of the photo-current occurred on the rear target surface with the return target current caused by electron emission from the target front side. Nonetheless, the low electrical conductivity of the irradiated PED target could cause the lowest value of the peak current in comparison with peak currents from metal target used in our experiment, compare Figs 6 and 8 with 9.

It is evident from Figs 2, 3, 6 and 8 that the targets loss electrons during the plasma expansion into the vacuum up to time
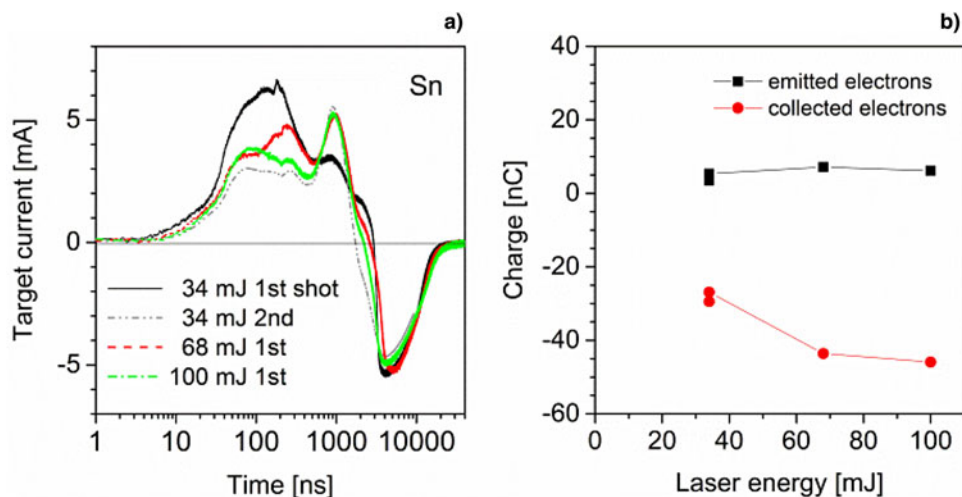

Fig. 8. Dependence of Sn-target current (a) and charge of electrons emitted and collected by target (b) on laser energy.

when the target polarization becomes negative due to the electrons coming from the vacuum chamber. The time instant t_{T-0}, where $I_T(t_{T-0})$ changes its sign depends not only on the target bulk material but also on the surface contamination level and on the laser intensity and fluence. Thus, the t_{T-0} indicates a critical change in the composition and movement of charged particles occurring in the vacuum chamber. One reason why the target polarization varies could be the fast rarefaction of the original laser-produced plasma and slow rarefaction of additionally ionized target vapor having nearly zero CM kinetic energy, while this energy of the plasma ions can reach a value of hundreds of eV (Krása *et al.*, 2011). Besides, the shape and size of the vacuum chamber affect the time-dependent behavior of the target polarization via the space–time nature of the laser-produced plasma. It is also evident that the duration of some tens microsecond of the afterglow phase can affect the process of laser ablation as well as observed mass spectra if a high-repetition rate scan is operated; in our experiment the repetition rate should lower than 30 kHz. One can achieve that the target polarization should be altered if the target material is converted to a plasma being mixed with a surrounding gas, as it applied in the laser ablation–inductively coupled plasma mass spectrometry (Russo *et al.*, 2013; Pozebon *et al.*, 2014).

4. CONCLUSIONS

The presented experimental study is devoted to the interaction of nanosecond pulsed lasers with metallic and plastic targets, as well as the resulting plasma formation and plume expansion which causes the polarization of targets. The results include the time-resolved measurement of the charge occurred in various targets, the influence of target surface impurities on the target current flowing between the target and ground, the analysis of the current balancing the target polarization, and the TOF and DOF spectra of ions expanding into the vacuum chamber, which are needed for the elucidation of specific time processes of the target polarization.

The similarity between the waveform shapes of observed target currents allows for revealing three phases in the development of the target polarization which is a global characteristic of the space–time changes in laser-produced plasma passing through the vacuum chamber:

(a) Ignition phase,
(b) Active phase,
(c) Afterglow phase.

The active phase and afterglow are crucial phenomena in the space–time development of the plasma produced by the laser ablation. These phases indicate different mechanisms for formation of ionized species in the laser ablation and subsequent processes during their expansion into the vacuum.

The duration of the positive polarization of various targets reaches a value of about 1 μs and it is much longer than the laser pulse duration $\tau_{FWHM} = 23$ ns for the KrF excimer laser experiment. In the case of the high-power laser pulses having $\tau_{FWHM} = 0.3$ ns, the active-phase duration is about 70 ns.

The afterglow phase characterized by the negative target polarization indicates two phenomena:

(c1) Formation of new structure and velocity distribution of the plasma at its edge impinging the target surface.
(c2) Ablated neutral species ionized by radiation leaving the laser-produced plasma can prevail over this plasma for a time of a few tens of microseconds.

This experiment confirms that laser-produced plasmas are extremely inhomogeneous at and after laser–matter interaction (Hora, 1991). The plasma inhomogeneities produce internal electric fields and currents which are formed by ionized species ablated from the target surface and target bulk. The analysis of target currents can reveal not only a shot-to-shot reproducibility of ablation, but also can provide approximate composition of the plasma expanding into a vacuum chamber, shape and sizes of which affect the target current at the late stage of the plasma expansion. Lastly, the target current can be used as a parameter of laser ablation.

REFERENCES

BENJAMIN, R.F., MCCALL, G.H. & EHLER, A.W. (1979). Measurement of return current in a laser-produced plasma. *Phys. Rev. Lett.* **42**, 890–893.

BOGAERTS, A., CHEN, Z., GIJBELS, R. & VERTES, A. (2003). Laser ablation for analytical sampling: what can we learn from modelling? *Spectrochim. Acta B* **58**, 1867–1893.

CIKHARDT, J., KRÁSA, J., DE MARCO, M., PFEIFER, M., VELYHAN, A., KROUSKÝ, E., CIKHARDTOVÁ, B., KLÍR, D., ŘEZÁČ, K., ULLSCHMIED, J., SKÁLA, J., KUBEŠ, P. & KRAVÁRIK, J. (2014). Measurement of the target current by inductive probe during laser interaction on terawatt laser system PALS. *Rev. Sci. Instrum.* **85**, 103507.

DE MARCO, M., KRÁSA, J., CIKHARDT, J., PFEIFER, M., KROUSKÝ, E., MARGARONE, D., AHMED, H., BORGHESI, M., KAR, S., GIUFFRIDA, L., VRANA, R., VELYHAN, A., LIMPOUCH, J., KORN, G., WEBER, S., VELARDI, L., DELLE SIDE, D., NASSISI, V. & ULLSCHMIED, J. (2016). Measurement of electromagnetic pulses generated during interactions of high power lasers with solid targets. *JINST* **11**, C06004.

DUBOIS, J.-L., LUBRANO-LAVADERCI, F., RAFFESTIN, D., RIBOLZI, J., GAZAVE, J., COMPANT LA FONTAINE, A., D'HUMIÈRES, E., HULIN, S., NICOLAÏ, PH., POYÉ, A. & TIKHONCHUK, V.T. (2014). Target charging in short-pulse-laser–plasma experiments. *Phys. Rev. E* **89**, 013102.

GIUFFREDA, E., DELLE SIDE, D., KRASA, J. & NASSISI, V. (2016). Polarization of plastic targets by laser ablation. *JINST* **11**, C05004.

HORA, H. (1991). *Plasmas at High Temperature and Density: Applications and Implications of Laser-Plasma Interaction, Lecture Notes in Physics, New Series m: Monographs*, ISBN 0-387-54312-0, New York Berlin Heidelberg: Springer-Verlag.

KRÁSA, J., DELLE SIDE, D., GIUFFREDA, E. & NASSISI, V. (2015). Characteristics of target polarization by laser ablation. *Laser Part. Beams* **33**, 601–605.

KRÁSA, J., LÁSKA, L., ROHLENA, K., VELYHAN, A., LORUSSO, A., NASSISI, V., CZARNECKA, A., PARYS, P., RYĆ, L. & WOLOWSKI, J. (2008). Effects of 2 mass % Si admixture in a laser-produced Fe plasma. *Appl. Phys. Lett.* **93**, 191503.

KRÁSA, J., LORUSSO, A., NASSISI, V., VELARDI, L. & VELYHAN, A. (2011). Revealing of hydrodynamic and electrostatic factors in the center-of-mass velocity of an expanding plasma generated by pulsed laser ablation. *Laser Part. Beams* **29**, 113–119.

KRÁSA, J., PARYS, P., VELARDY, L., VELYHAN, A., DELLE SIDE, D. & NASSISI, V. (2014). Time-of-flight spectra for mapping of charge density of ions produced by laser. *Laser Part. Beams* **32**, 15–20.

MORA, P. (2003). Plasma expansion into a vacuum. *Phys. Rev. Lett.* **90**, 185002.

POYÈ, A., DUBOIS, J.-L., LUBRANO-LAVADERCI, F., D'HUMIÀRES, E., BARDON, M., HULIN, S., BAILLY-GRANDVAUX, M., RIBOLZI, J., RAFFESTIN, D., SANTOS, J.J., NICOLAÏ, PH. & TIKHONCHUK, V. (2015). Dynamic model of target charging by short laser pulse interactions. *Phys. Rev. E* **92**, 043107.

POZEBON, D., SCHEFFLER, G.L., DRESSLER, V.L. & NUNES, M.A.G. (2014). Review of the applications of laser ablation inductively coupled plasma mass spectrometry (LA-ICP-MS) to the analysis of biological samples. *J. Anal. At. Spectrom.* **29**, 2204–2228.

RUSSO, R.E., MAO, X., GONZALEZ, J.J., ZORBA, V. & YOO, J. (2013). Laser ablation in analytical chemistry. *Anal. Chem.* **85**, 6162–6177.

WEAVER, I., MARTIN, G.W., GRAHAM, W.G., MORROW, T. & LEWIS, C.L.S. (1999). The Langmuir probe as a diagnostic of the electron component within low temperature laser ablated plasma plumes. *Rev. Sci. Instrum.* **70**, 1801–1805.